The pulvinar regulates plasticity in human visual cortex

Miriam Acquafredda[1], Jan W. Kurzawski[2], Laura Biagi[3], Michela Tosetti[3,4], Maria Concetta Morrone[1], Paola Binda[1]

[1] University of Pisa, Italy

[2] Maastricht University, Maastricht, Netherlands

[3] IRCCS Stella Maris, Calambrone, Pisa, Italy

[4] IMAGO Center, Pisa, Italy

Abstract

In normally sighted human adults, two-hours of monocular deprivation is sufficient to transiently alter ocular dominance. Here we show that this is associated with a reduction of functional connectivity between the pulvinar and early visual cortex, selective for the pulvinar-to-V1 directionality. Our results support a revised model of adult V1 plasticity, where short-term reorganization is gated by modulatory signals relayed by the pulvinar.

Introduction

The potential for long-term plastic change in the sensory brain declines with age, probably through active stabilization of the sensory circuitry[1]. Nevertheless, adult sensory systems retain the potential for short-term plasticity[2,3]: blocking vision in one eye for a few hours in human adults induces a transient boost of the deprived eye[4,5]. This homeostatic response reflects a gain-change of the deprived eye representation, which could serve to counterbalance the reduced stimulation[6]. However, there is recent evidence that the same boost can be achieved without blocking stimulation of either eye, merely manipulating attention and multimodal context[7-10]. This suggests a radically novel interpretation of adult plasticity, where top-down multimodal signals play a key role.

One main pathway through which multimodal signals reach the primary visual cortex (V1) is via the thalamic nucleus pulvinar, which modulates V1 activity through recurrent cortico-thalamo-cortical loops[11,12]. These loops connect distant sensory, motor and cognitive areas and may underly predictive coding[13-15]: by collecting multimodal signals, the pulvinar may carry predictions about the upcoming sensory events to low-level sensory areas, including V1[16,17]. In line with this model, there is evidence that reducing the pulvinar influence over V1 permits the updating of perceptual representations, i.e. perceptual learning[18].

Based on this evidence, we hypothesize that the pulvinar exerts a stabilizing influence over the primary sensory cortex, and that reducing this influence may open an opportunity for plasticity – even for a very stable property like ocular dominance. To test this idea, we used high resolution 7T-fMRI and asked whether short-term monocular deprivation impacts the pulvinar-V1 connectivity.

Methods

Experimental model and study participant details

Experimental procedures are in line with the principles of the declaration of Helsinki and were approved by the regional ethics committee [Comitato Etico Pediatrico Regionale—Azienda Ospedaliero-Universitaria Meyer—Firenze (FI)] and by the Italian Ministry of Health, under the protocol 'Plasticità e multimodalità delle prime aree visive: studio in risonanza magnetica a campo ultra alto (7T)' version #1 dated 11/11/2015. Written informed consent was obtained from each participant, which included consent to process and preserve the data and publish them in anonymous form. We analyzed data from two fMRI sessions, acquired before and after two hours of monocular deprivation. Twenty-five healthy volunteers with normal or corrected-to-normal visual acuity were tested. Sample size was set based on the minimum number of participants (N = 18) required to reliably detect a medium sized effect of monocular deprivation on fMRI signals[33,34]. Due to image distortions, data from 3 and 6 participants were discarded from the first (TR = 3s) and second (TR = 1s) fMRI dataset. This left respectively 22 participants for the TR = 3s fMRI dataset (12 females mean age ± S.E.M.= 26.5 ± 0.82, also included in the analyses of the DWI dataset) and 19 participants for the TR = 1s fMRI dataset (12 females, mean age ± S.E.M.= 26.5 ± 0.84).

Method details

Short-term monocular deprivation

Monocular deprivation was achieved by patching the dominant eye for two hours. Like in previous studies[5,33], we used a translucent eye-patch made of plastic material allowing light to reach the retina (luminance attenuation 0.07 logUnits). During the monocular deprivation, participants were free to walk, read and use a computer, but they did not eat nor sleep.

Binocular rivalry

Ocular dominance changes (before vs. after deprivation) were evaluated with two brief binocular rivalry sessions, each comprising two 3-minute runs, immediately prior to each fMRI

session. The visual stimuli were presented on a 15-inch LCD monitor viewed from 57 cm through anaglyph goggles (blue filter on the right lens, red filter on the left). The stimuli consisted of two oblique gratings (red and blue), oriented at ±45°, measuring 3° in diameter, with a spatial frequency of 2 cycles per degree (cpd) and 50% contrast. Equiluminance between the red and the blue gratings was achieved by reducing the intensity of the red channel based on photometric measurements (mean luminance of both the red and blue grating: 1.8 cd/m2). The dichoptic gratings were surrounded by a binocular sharp-edged white frame (encouraging fusion) and displayed against a uniform black background. During the experiment, participants continuously reported their perception by keeping one of three keys pressed: right or left arrows to report dominance of the clockwise or counter-clockwise oblique gratings; down-arrow key to report mixed percepts. Dominance phase durations shorter than 0.3 seconds (finger errors) and longer than 30 seconds (failed rivalry) were discarded. The dominant eye was defined as the eye showing the longer mean phase duration during the baseline binocular rivalry measurements.

We defined ocular dominance as the total time during which the stimulus presented in the dominant eye was perceived, divided by the total time during which the stimulus in either eye was perceived (which amounts to the total testing time minus the time during which a mixture of the two stimuli was perceived):

$$ODI = \left(\frac{TimeDE}{TimeDE + TimeNDE}\right) * 100 \qquad \text{(Equation 1)}$$

where ODI stands for Ocular Dominance Index, DE for dominant eye and NDE for non-dominant eye. The effect of monocular deprivation was quantified as the ODI difference before and after the two-hour deprivation.

MR system and sequences

Scanning was performed on a 7T-MRI system (SIGNA7T-PISA, GE Healthcare, Milwaukee, WI, USA) equipped with a 2-channel transmit and a 32-channel receiver head-coil (Nova Medical, Wilmington, MA, USA).

Anatomical images were acquired at 0.8 mm isotropic resolution using a MP-RAGE (Magnetization Prepared RApid Gradient Echo) sequence with the following parameters: echo time TE = 3.5 ms, GRE repetition time TR_{GRE} = 7.3 ms, repetition time TR_{MPRAGE} = 3380 ms, inversion time TI = 1100 ms, delay time TD = 1600 ms, flip angle FA = 8°, rBW = 62.5 kHz, field of view FOV = 220 mm, matrix = 276x276, slice thickness = 0.8mm, 200 slices.

Two sets of functional MR images were acquired at the same isotropic spatial resolution of 1.5 mm (matrix = 128x128, slice thickness = 1.4 mm, slice spacing = 0.1 mm), rBW = 250 kHz, FA=77°, ASSET = 2, phase encoding direction Anterior-to-Posterior (AP).

The first fMRI dataset had TR = 3000 ms, TE = 23 ms, number of volumes = 160.

The second fMRI dataset had TR = 1000 ms, TE = 19.3 ms, number of volumes = 300.

Each functional sequence included 4 initial dummy volumes, to allow the stationarity of the signal. For each EPI sequence, we acquired four additional volumes with the reversed phase encoding direction (Posterior-to-Anterior, PA), used for distortion correction. We acquired each set of functional images (TR = 3s first, followed by TR = 1s) in resting-state with eyes closed.

For the study of structural connectivity, Diffusion Weighted Imaging (DWI) datasets were acquired by using a MUltiplexed Sensitivity-Encoding (MUSE) sequence with 2 mm isotropic resolution (FOV = 200 mm, matrix =100x100, slice thickness = 2 mm). The other acquisition parameters were: TR = 5500 ms, TE = 50.5 ms, 2 echoes, ASSET = 2, 32 noncollinear diffusion gradient directions with b-value of 1000 s/mm^2, four volumes without b-value = 0 s/mm^2.

MRI preprocessing

Preprocessing of anatomical and functional MR images was performed with BrainVoyager[35] (version 20.6), Freesurfer[36] (v6.0.0), FSL[37] (version 6.0.4) and ANTs[38]. In addition, Matlab (The MathWorks Inc.) was used to perform resting-state analyses.

Anatomical images were processed by a standard procedure for segmentation implemented in Freesurfer (recon-all[36]). Transformation matrices from individual participants' T1 anatomical images to the MNI template[39] were computed through an affine registration and a warping procedure using the antsRegistrationSyN.sh routine[38].

fMR images were corrected for slice time and motion[35] and undistorted using EPI images with reversed phase encoding direction, using the Brain Voyager COPE plug-in[40]. We then exported the preprocessed images from BrainVoyager to NiFTi format. Each participants' first functional acquisition (acquired right after the anatomical images) was aligned to the corresponding anatomy using a boundary based registration algorithm (Freesurfer bbergister function). All functional volumes were aligned to the same first functional acquisition with a rigid transformation (using antsRegistrationSyN.sh and antsApplyTransforms.sh), then registered to the MNI space using the affine transformation and warp fields obtained from the anatomical registration (described above, matrices applied with antsApplyTransforms.sh).

fMR images with TR = 3s were preprocessed as follows. After slice-time and motion correction, the fMRI time-series were band-pass temporal filtered (0.01– 0.1 Hz, minimum-order filter with a stopband attenuation of 60 dB); to minimize filtering artifacts, we excluded the first and last 5 TRs from further analysis. Next, we regressed out three main potential confounds (modelled by 14 regressors), as in previous work on pulvino-cortical interactions[11]: (1) the six motion-parameter estimates and their temporal derivatives, (2) the signal from the three ventricular spaces (average signal in the first, second and third ventricles, defined by the recon-all routine[36]) and (3) the signal from the cerebral white matter (defined by the Harvard-Oxford subcortical atlas[41]).

fMR images with TR = 1s were preprocessed in a similar way. After slice-time and motion correction, the fMRI time-series were high-pass temporal filtered (0.0078 Hz, minimum-order filter with a stopband attenuation of 60 dB); to minimize filtering artifacts, we excluded the first and last 5 TRs from further analysis. Next, we regressed out three main potential confounds (modelled by 20 regressors): (1) the physiological parameters (respiration and cardiac pulsation preprocessed with the PhysIO Toolbox[42]), (2) the signal from the three ventricular spaces (average signal in the first, second and third ventricles, defined by the recon-all routine[36]) and (3) the signal from the cerebral white matter (defined by the Harvard-Oxford subcortical atlas[41]).

Diffusion weighted images (DWI) were preprocessed with QSIprep[43]. Preprocessing involved distortion correction, denoising using MP-PCA, motion correction and registration to anatomical template. Tensor fitting and reconstruction of the whole brain tractogram was performed with pyAFQ. The tractogram was generated with 1500000 seeds using a CSD model and was limited by a white matter mask. Optic radiations and pulvinar-V1 radiations were segmented based on LGN, pulvinar and V1 masks imported in pyAFQ. After successfully labelling tracts belonging to the optic radiation, outlier tracts were removed as a part of pyAFQ cleaning pipeline. Fractional Anisotropy (FA) profiles for clean bundles were generated after resampling the tract length at 100 points. For each participant we estimated the FA profiles before and after monocular deprivation and compared them with paired t-tests. The associated two-tailed p-values were evaluated against an FDR[44] corrected 0.05 threshold.

Quantification and statistical analysis

Functional connectivity analysis

Functional connectivity was estimated with both a within-participant and an aggregated subject approach. For the within-participant approach, we computed the Pearson's correlation coefficient between the fMRI time-series in pairs of ROIs (average time-series of all voxels within the ROI). The correlation coefficients were Fisher-transformed to ensure normality; the resulting values were compared before vs. after monocular deprivation using paired t-tests (two-sided p-values).

With the aggregate subject approach, we generated functional connectivity maps over the whole cortical surface. For this, we concatenated the z-scored individual participant's fMRI time-series and computed the Pearson's correlation between the average time-series in each ROI and the time-series of each cortical voxels. We also computed voxel-wise differences of Pearson's correlation coefficients before and after deprivation. We mapped the three coefficients (correlations before and after deprivation, and correlation differences across deprivation) on a 3D rendering of the cortical surface (fsaverage) and applied a spatial smoothing (FWHM = 3 mm). The two hemispheres were then registered to the same symmetric surface (fsaverage_sym) and the two correlation maps averaged. The individual vertex correlation coefficients were associated with two-sided p-values via Studentization (for the pre and post-deprivation values) or using Fisher transformation (for the post-pre differences). The resulting surface maps (shown in Figure 1 and Extended Data Figure 1 and 2) were thresholded after FDR[44] correction of the two-sided p-values (FDR-corrected thresholds for the pulvinar ROI: $p_{pre} = 2.90 \times 10^{-3}$; $p_{post} = 2.80 \times 10^{-3}$; $p_{difference} = 1.45 \times 10^{-4}$; LGN: $p_{pre} = 1.80 \times 10^{-3}$; $p_{post} = 1.40 \times 10^{-3}$; $p_{difference}$= NaN, meaning that no voxel passed the threshold; V1: $p_{pre} = 3.00 \times 10^{-3}$; $p_{post} = 2.6 \times 10^{-3}$; $p_{difference} = 3.68 \times 10^{-5}$) and cluster corrected (cluster size = 50 vertices). We also visualized volume maps (Figure 2), where correlations values before and after deprivation were thesholded after FDR[44] correction of the p-values (thresholds: $p_{pre} = 9.87 \times 10^{-6}$, $p_{post} = 9.87 \times 10^{-6}$; no cluster correction).

Effective connectivity analysis

From the high-temporal resolution fMR images (TR = 1s, average time-series of all voxels within the pulvinar, LGN and V1 ROIs), we estimated effective connectivity with a within-subjects approach using dynamic causal modeling[23] in the rDCM toolbox implementation[45,46]

(available as part of the TAPAS software collection[47]). The rDCM routine returned parameter estimates for the fully connected network, i.e. bidirectional connections between pulvinar and V1, LGN and V1 and between pulvinar and LGN (the "A-matrix"). The significance of the individual connections was assessed with one-sample t-tests across participants and the associated two-tailed p-values were evaluated against an FDR[44] corrected 0.05 threshold.

We further tested the effect of monocular deprivation on effective connectivity with a two-by-two ANOVA for repeated measures, with main factors time (before and after deprivation) and directionality (e.g., pulvinar-to-V1 and V1-to-pulvinar). This was followed up with post-hoc t-tests, and the associated two-tailed p-values were evaluated against an FDR[44] corrected 0.05 threshold.

We complemented this DCM analysis with a simpler cross-correlation of the same fMRI time-series. This was implemented with the standard xcorr Matlab function set to the "normalize" option, which returned cross-correlation coefficients normalized by the autocorrelations. To test whether the asymmetry of the curves changed after deprivation, we took the average cross-correlation at the three negative and positive lags closest to zero ([-3 -2 -1] and [+1 +2 +3]) and evaluated their difference before vs. after deprivation with a series of paired t-tests across participants. The associated two-tailed p-values were evaluated against an FDR[44] corrected 0.05 threshold.

ROI definition

All ROIs were defined in the MNI space, to which our functional scans were registered. For each subject and fMRI acquisition, we extracted the average BOLD signal from all voxels within the ROI (using the fslmeants function).

The pulvinar ROI was taken from a published atlas[19] defined from Diffusion-Weighted Images. The Lateral Geniculate Nucleus (LGN) was taken from the NSD dataset, which outlined it based on a combination of functional data (retinotopic mapping experiments) constrained with anatomical features[22].

The V1 ROI was taken from the Glasser cortical parcellation atlas[21], defined in the fsaverage surface space, and projected to the MNI volume (https://identifiers.org/neurovault.collection:1549).

Results

We first confirmed the deprivation effect in 22 normally sighted adults. After the two-hour monocular deprivation, ocular dominance, measured with a short binocular rivalry test immediately before MRI scanning, shifted in favor of the deprived eye by 9% (from 55% to 64% dominance; $|t_{(21)}| = 6.76$, $p < 0.001$).

Next we measured the resting-state (eyes closed) functional connectivity between the pulvinar (atlas-based ROI definition[19]) and the cortex; this was strong in all sensory regions, including occipital visual areas, temporal auditory areas and central somatosensory areas (Figure 1A), consistent with the multimodality of the pulvinar[20]. After monocular deprivation, there was a dramatic reduction of pulvinar connectivity with the occipital cortex, including the primary visual cortex V1 and surrounding early visual areas.

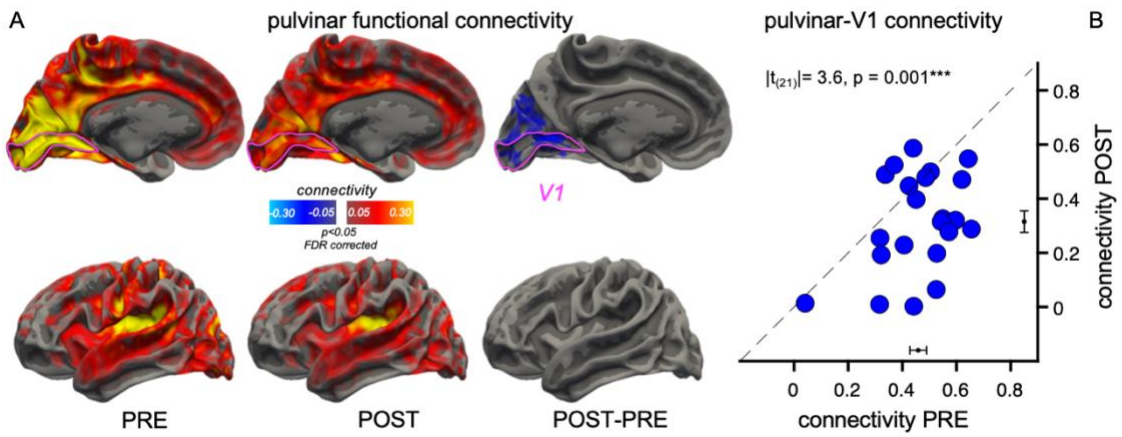

Figure 1. Functional connectivity of the pulvinar, measured with resting-state 7T-fMRI

A: Functional connectivity of the pulvinar, estimated from resting-state fMRI (TR = 3s, full brain coverage) and mapped over the cortical surface (medial and lateral view; maps are averaged across hemispheres and projected on a symmetrical template of the cortical surface). The leftmost and central maps show the connectivity before and after two hours of monocular deprivation; the rightmost maps show the connectivity change, showing significant reductions in most early visual areas; there was also a connectivity reduction in two small areas of the superior temporal gyrus and the central sulcus; these are not visible in this projection (they are in the alternative projection in Fig. S2B). Connectivity was estimated as the Pearson's r coefficient between the fMRI timeseries in the pulvinar and the time-series of each cortical voxel, computed after nuisance regression and concatenation across N=22 participants. Maps are thresholded at $|r| > 0.05$ an $p < 0.05$ FDR corrected, and cluster corrected (50 vertices).

B: Functional connectivity between the pulvinar and V1 (atlas-based definition, see pink outline in Panel A) before and after deprivation, for the individual participants. Pearson's r values were Fisher transformed to allow for statistical comparisons; the black error bars near the axes show the mean +/- S.E.M. connectivity: 0.50 ±0.04 before deprivation reduces to 0.34

± 0.04 after deprivation. The text inset reports the results of the paired t-test comparing functional connectivity before and after deprivation (Cohen's d = 0.80).

This connectivity reduction after deprivation was confirmed by calculating functional connectivity for the individual participants, from the average time series of two a-priori selected Regions of Interest: pulvinar[19] and V1[21] (Figure 1B). In contrast, no connectivity change was observed between LGN[22] and V1[21] (Supplementary Fig. S1A-B), nor between V1 and the other occipital areas (Supplementary Fig. S2A). There was, however, a reduction of V1 connectivity with high-level areas including the superior temporal gyrus, the intraparietal sulcus, the premotor cortex and the cingulate gyrus (Supplementary Fig. 2A).

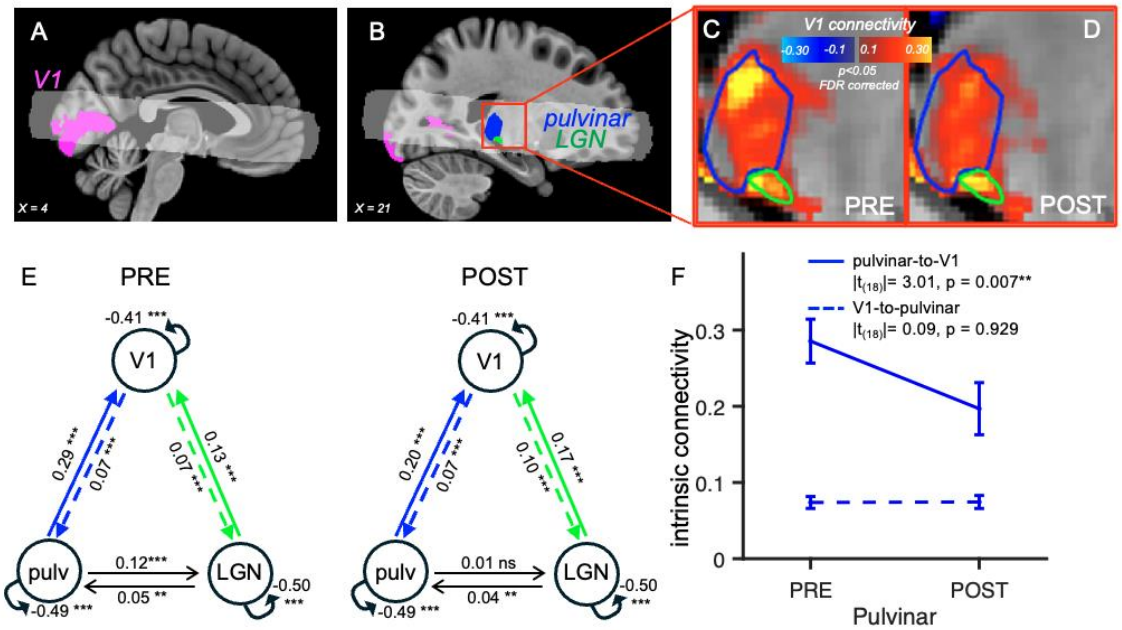

Figure 2. Thalamus-V1 functional connectivity and effective connectivity measured with Dynamic Causal Modelling of the resting-state 7T-fMRI time-series

A-B: Partial volume covered by a high-temporal resolution fMRI (TR = 1s, partial volume: white shading shows spatial coverage across 50% of our acquisitions) used for measuring connectivity between V1 (defined as the intersection between the atlas-based V1 region of interest[21], in pink, and the coverage afforded by our sequence) and the thalamic regions pulvinar and LGN (atlas-based definitions[19,22], blue and green masks), visualized in two different sagittal slices (x-MNI coordinates shown as text insets).

C-D: Functional connectivity between V1 and the thalamus (measured with high-temporal resolution fMRI depicted in panels A-B), before and after monocular deprivation. Blue and green outlines mark the borders of the pulvinar and LGN ROIs. Connectivity was estimated as the Pearson's r coefficient between the fMRI time-series in V1 and the timeseries of each voxel

in the thalamus, computed after nuisance regression and concatenation across N=19 participants; maps are thresholded at |r| > 0.05 an p < 0.05 FDR corrected.

*E: Average effective connectivity across subjects in the network including V1, pulvinar, LGN; continuous colored lines mark connections from the thalamus to V1, dashed colored lines from V1 to the thalamus. Numbers show intrinsic connectivity (A-matrix in rDCM) and associated statistical significance (after FDR correction: *** for p < 0.001, ** for p < 0.01, * for p < 0.05, ns for p >= 0.05), independently estimated before and after monocular deprivation.*

*F: Change of effective connectivity between the pulvinar and V1, shown as mean (same numbers as in E) and S.E.M across participants. A 2x2 ANOVA with factors time (pre vs. post deprivation) and directionality (pulvinar-to-V1 vs. V1-to-pulvinar) showed a significant interaction (F (1,18) = 12.2, p = 0.002, $\eta^2_{partial}$ = 0.35). Text insets report the post-hoc t-tests comparing effective connectivity values before and after deprivation for the two directionalities (after FDR correction: **p < 0.01, * p < 0.05; Cohen's d = 0.69 and 0.02 for pulvinar-to-V1 and V1-to-pulvinar respectively). Monocular deprivation also affected the intrinsic connectivity between pulvinar and LGN (2x2 ANOVA: F (1,18) = 4.9, p = 0.039, $\eta^2_{partial}$ = 0.22), with a significant decrease of pulvinar-to-LGN connectivity ($|t_{(18)}|$= 2.62, p = 0.017, Cohen's d = 0.60), and unaffected LGN-to-pulvinar connectivity ($|t_{(18)}|$= 0.69, p = 0.500, Cohen's d = 0.16).*

To estimate the directionality of the pulvinar-V1 connectivity change (feedforward vs. feedback), we acquired a second resting-state fMRI dataset, with higher temporal resolution (TR = 1 second, covering V1 and the thalamus, Figure 2A-B). The V1 functional connectivity map shows two foci within the thalamus (Figure 2C): one (dorsal) falling within the atlas-based definition of the pulvinar[19], and the other (ventral) within the atlas-based definition of LGN[22]. Comparison of the V1 connectivity map before and after deprivation (Figure 2C-D) suggests a selective reduction in the pulvinar, but not LGN. Effective connectivity estimates from Dynamic Causal Modelling[23] on the individual participants' data (Figure 2E-F) shows that monocular deprivation selectively reduced the pulvinar-to-V1 connectivity (and pulvinar-to-LGN connectivity), leaving the LGN-to-V1 connectivity (and the LGN-to-pulvinar connectivity) unaffected. In contrast, the V1-to-thalamus connectivity was not affected. These DCM-based conclusions are supported by a simpler cross-correlation analysis of the BOLD timeseries (Supplementary Figure S3).

We also assessed whether these functional connectivity changes are associated with changes in structural connectivity. We acquired Diffusion-Weighted MR Images during the same sessions as the resting-state scans. Figure 3 shows that thalamus-V1 structural connectivity was unaffected by monocular deprivation.

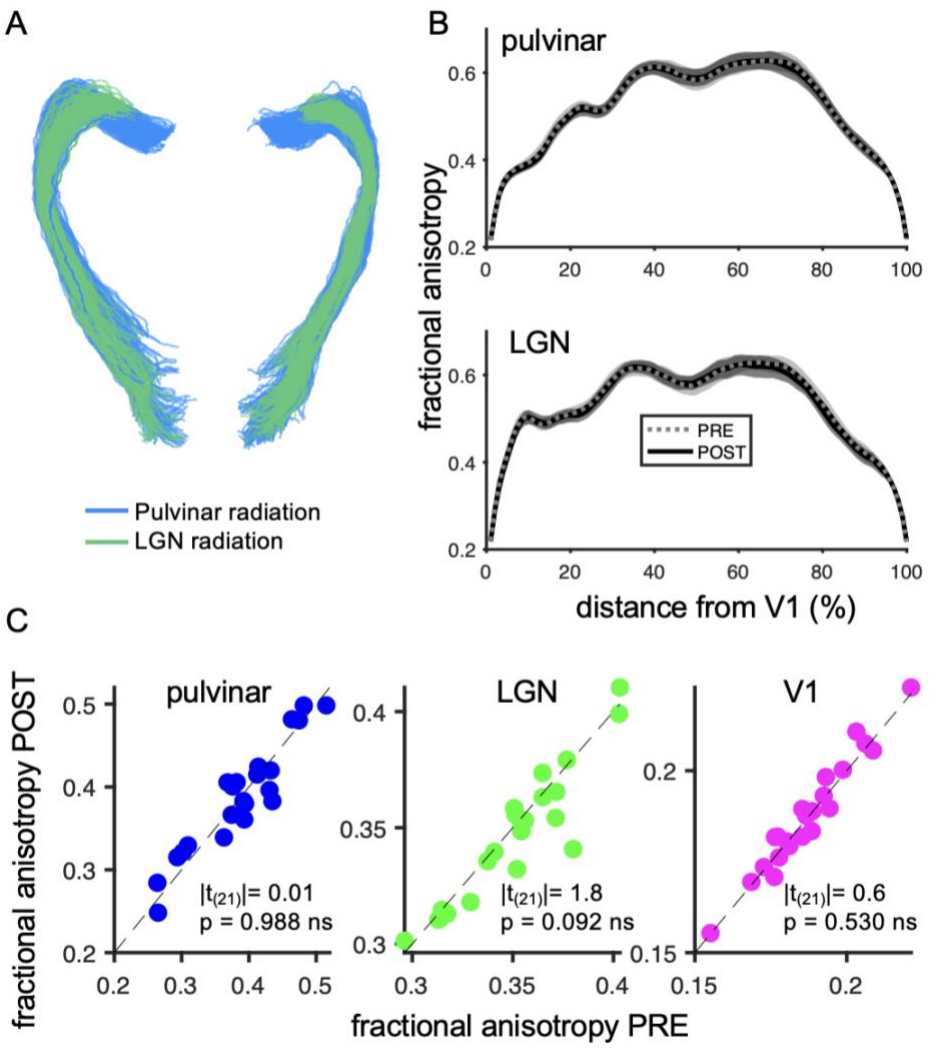

Figure 3. Structural connectivity between the thalamus and V1, measured with Diffusion Weighted Imaging

A: Fiber-tracking (visualized in DSI-STUDIO) for a representative participant, mapping the structural connectivity between V1 and two thalamic regions: LGN and pulvinar.

B: Fractional anisotropy values as a function of nodes along the tracts (averaged across hemispheres), measured before (dashed gray lines) and after monocular deprivation (continuous black lines); shaded areas show 1 S.E.M. across participants. No difference was detected before vs. after monocular deprivation (paired t-tests, all $p > 0.05$ FDR corrected).

C: Fractional anisotropy before vs. after monocular deprivation within each region, for the individual participants. Text insets report the results of paired t-tests comparing fractional anisotropy before and after deprivation (Cohen's $d = 0.00$, 0.38 and 0.14 for pulvinar, LGN and V1).

Discussion

In summary, our results show that two-hours of monocular deprivation reshapes the reciprocal interactions between visual brain regions, decreasing the influence of the pulvinar on resting-state V1 activity. In contrast, monocular deprivation does not reduce the LGN bottom-up sensory drive to V1.

Given that pulvinar-to-V1 projections can exert an inhibitory effect[24], the reduced pulvinar connectivity is consistent with the evidence that monocular deprivation reduces resting GABA in V1[25]. A down-weighting of pulvinar inputs to V1 may be a common trait of diverse adult V1 plasticity phenomena, including monocular deprivation and perceptual learning, as both are associated with reduced pulvinar-V1 connectivity and decreased cortical GABA[18,25]. While perceptual learning is accompanied by structural plasticity[18] (like motor learning[26]), we found that monocular deprivation does not affect structural connectivity (assessed through DWI). This suggests that structural plasticity may require a longer period of altered experience than the mere two hours of our deprivation.

Monocular deprivation is often interpreted as a homeostatic response to the reduced sensory input in one eye[6]. However, local V1 modulations cannot explain the reorganization of thalamo-cortical functional connectivity, specific to the pulvinar, which we report here. Since the pulvinar is crucial for conveying multimodal modulatory inputs to early sensory areas[13,14,16], we suggest that a primary effect of monocular deprivation is to reduce the impact of top-down signals on early visual processing. This is in line with previous evidence of impaired multisensory integration[27] and reduced feedback signaling (alpha rhythms)[28,29] after monocular deprivation. The reduction of top-down influences could result from the sensory conflict generated by deprivation, as the occluded eye fails to signal events carried by the other senses. A similar effect would be achieved by distorting the monocular image[30], applying a monocular inverting prism[7], or monocular delay[8], all of which introduce a sensory conflict and mimic the effects of monocular deprivation, despite leaving the strength of the visual stimulation unaltered. Repeated incongruence reduces the integration weights assigned to multisensory signals, thereby allowing for sensory recalibration[31]. On this view, ocular dominance plasticity in adults may be re-interpreted as a recalibration response, triggered by the reduced top-down modulatory inputs conveyed by the pulvinar to V1. This perspective is in line with suggestions that the pulvinar plays a key role in cortical plasticity and the reshaping of functional organization in the visual cortex[32].

To conclude, our results stimulate a new understanding of short-term monocular deprivation effects, which goes beyond local gain-changes of evoked V1 responses, pointing to a functional

reorganization of the visual processing network. We speculate that experience-dependent changes in early visual cortex depend on reducing the multimodal influences conveyed by the pulvinar, implying that the pulvinar may be the gatekeeper of adult sensory plasticity.

Acknowledgements

This research was funded by: the European Research Council (ERC) under the Horizon EU framework, Consolidator grant PREDACTIVE (n. 101170249); the European Union - Next Generation EU, in the context of The National Recovery and Resilience Plan, Investment 1.5 Ecosystems of Innovation, Project Tuscany Health Ecosystem (THE, CUP I53C22000780001), and of the grant PRIN 2022 (Project 'RIGHTSTRESS—Tuning arousal for optimal perception', Grant no. 2022CCPJ3J, CUP I53D23003960006); and by the Italian Ministry of University and Research under the program FARE-2 (grant SMILY). The work of LB and MT is supported by the Italian Ministry of Health, via RC 2025 to IRCCS Fondazione Stella Maris. The authors would like to thank Paolo Bosco for help with data preprocessing, and David C. Burr for his comments on the manuscript.

Declaration of interests

The authors declare no competing interests.

References

1. Espinosa, J.S., and Stryker, M.P. (2012). Development and plasticity of the primary visual cortex. Neuron *75*, 230-249. 10.1016/j.neuron.2012.06.009.
2. Sawtell, N.B., Frenkel, M.Y., Philpot, B.D., Nakazawa, K., Tonegawa, S., and Bear, M.F. (2003). NMDA receptor-dependent ocular dominance plasticity in adult visual cortex. Neuron *38*, 977-985. 10.1016/s0896-6273(03)00323-4.
3. Hofer, S.B., Mrsic-Flogel, T.D., Bonhoeffer, T., and Hubener, M. (2006). Prior experience enhances plasticity in adult visual cortex. Nat Neurosci *9*, 127-132. 10.1038/nn1610.
4. Zhou, J., Clavagnier, S., and Hess, R.F. (2013). Short-term monocular deprivation strengthens the patched eye's contribution to binocular combination. J Vis *13*. 10.1167/13.5.12.
5. Lunghi, C., Burr, D.C., and Morrone, C. (2011). Brief periods of monocular deprivation disrupt ocular balance in human adult visual cortex. Curr Biol *21*, R538-539. 10.1016/j.cub.2011.06.004.
6. Castaldi, E., Lunghi, C., and Morrone, M.C. (2020). Neuroplasticity in adult human visual cortex. Neurosci Biobehav Rev *112*, 542-552. 10.1016/j.neubiorev.2020.02.028.
7. Wang, M., McGraw, P., and Ledgeway, T. (2021). Attentional eye selection modulates sensory eye dominance. Vision Res *188*, 10-25. 10.1016/j.visres.2021.06.006.

8. Steinwurzel, C., Morrone, M.C., Sandini, G., and Binda, P. (2023). Active vision gates ocular dominance plasticity in human adults. Curr Biol *33*, R1038-R1040. 10.1016/j.cub.2023.08.062.
9. Song, F., Lyu, L., Zhao, J., and Bao, M. (2023). The role of eye-specific attention in ocular dominance plasticity. Cereb Cortex *33*, 983-996. 10.1093/cercor/bhac116.
10. Kim, H.W., Kim, C.Y., and Blake, R. (2017). Monocular Perceptual Deprivation from Interocular Suppression Temporarily Imbalances Ocular Dominance. Curr Biol *27*, 884-889. 10.1016/j.cub.2017.01.063.
11. Arcaro, M.J., Pinsk, M.A., Chen, J., and Kastner, S. (2018). Organizing principles of pulvino-cortical functional coupling in humans. Nat Commun *9*, 5382. 10.1038/s41467-018-07725-6.
12. Sherman, S.M., and Usrey, W.M. (2024). Transthalamic Pathways for Cortical Function. J Neurosci *44*. 10.1523/JNEUROSCI.0909-24.2024.
13. Kanai, R., Komura, Y., Shipp, S., and Friston, K. (2015). Cerebral hierarchies: predictive processing, precision and the pulvinar. Philos Trans R Soc Lond B Biol Sci *370*. 10.1098/rstb.2014.0169.
14. Bastos, A.M., Usrey, W.M., Adams, R.A., Mangun, G.R., Fries, P., and Friston, K.J. (2012). Canonical microcircuits for predictive coding. Neuron *76*, 695-711. 10.1016/j.neuron.2012.10.038.
15. de Lange, F.P., Heilbron, M., and Kok, P. (2018). How Do Expectations Shape Perception? Trends Cogn Sci *22*, 764-779. 10.1016/j.tics.2018.06.002.
16. Miura, S.K., and Scanziani, M. (2022). Distinguishing externally from saccade-induced motion in visual cortex. Nature *610*, 135-142. 10.1038/s41586-022-05196-w.
17. Kastner, S., Fiebelkorn, I.C., and Eradath, M.K. (2020). Dynamic pulvino-cortical interactions in the primate attention network. Curr Opin Neurobiol *65*, 10-19. 10.1016/j.conb.2020.08.002.
18. Ziminski, J.J., Frangou, P., Karlaftis, V.M., Emir, U., and Kourtzi, Z. (2023). Microstructural and neurochemical plasticity mechanisms interact to enhance human perceptual decision-making. PLoS Biol *21*, e3002029. 10.1371/journal.pbio.3002029.
19. Najdenovska, E., Aleman-Gomez, Y., Battistella, G., Descoteaux, M., Hagmann, P., Jacquemont, S., Maeder, P., Thiran, J.P., Fornari, E., and Bach Cuadra, M. (2018). In-vivo probabilistic atlas of human thalamic nuclei based on diffusion- weighted magnetic resonance imaging. Sci Data *5*, 180270. 10.1038/sdata.2018.270.
20. Froesel, M., Cappe, C., and Ben Hamed, S. (2021). A multisensory perspective onto primate pulvinar functions. Neurosci Biobehav Rev *125*, 231-243. 10.1016/j.neubiorev.2021.02.043.
21. Glasser, M.F., Coalson, T.S., Robinson, E.C., Hacker, C.D., Harwell, J., Yacoub, E., Ugurbil, K., Andersson, J., Beckmann, C.F., Jenkinson, M., et al. (2016). A multi-modal parcellation of human cerebral cortex. Nature *536*, 171-178. 10.1038/nature18933.
22. Allen, E.J., St-Yves, G., Wu, Y., Breedlove, J.L., Prince, J.S., Dowdle, L.T., Nau, M., Caron, B., Pestilli, F., Charest, I., et al. (2022). A massive 7T fMRI dataset to bridge cognitive neuroscience and artificial intelligence. Nat Neurosci *25*, 116-126. 10.1038/s41593-021-00962-x.
23. Friston, K.J., Harrison, L., and Penny, W. (2003). Dynamic causal modelling. Neuroimage *19*, 1273-1302. 10.1016/s1053-8119(03)00202-7.
24. Fang, Q., Chou, X.L., Peng, B., Zhong, W., Zhang, L.I., and Tao, H.W. (2020). A Differential Circuit via Retino-Colliculo-Pulvinar Pathway Enhances Feature Selectivity in Visual Cortex through Surround Suppression. Neuron *105*, 355-369 e356. 10.1016/j.neuron.2019.10.027.

25. Lunghi, C., Emir, U.E., Morrone, M.C., and Bridge, H. (2015). Short-term monocular deprivation alters GABA in the adult human visual cortex. Curr Biol *25*, 1496-1501. 10.1016/j.cub.2015.04.021.
26. Lazari, A., Salvan, P., Cottaar, M., Papp, D., Rushworth, M.F.S., and Johansen-Berg, H. (2022). Hebbian activity-dependent plasticity in white matter. Cell Rep *39*, 110951. 10.1016/j.celrep.2022.110951.
27. Lo Verde, L., Morrone, M.C., and Lunghi, C. (2017). Early Cross-modal Plasticity in Adults. J Cogn Neurosci *29*, 520-529. 10.1162/jocn_a_01067.
28. Federici, A., Bernardi, G., Senna, I., Fantoni, M., Ernst, M.O., Ricciardi, E., and Bottari, D. (2023). Crossmodal plasticity following short-term monocular deprivation. Neuroimage *274*, 120141. 10.1016/j.neuroimage.2023.120141.
29. Lunghi, C., Berchicci, M., Morrone, M.C., and Di Russo, F. (2015). Short-term monocular deprivation alters early components of visual evoked potentials. J Physiol *593*, 4361-4372. 10.1113/JP270950.
30. Ramamurthy, M., and Blaser, E. (2018). Assessing the kaleidoscope of monocular deprivation effects. J Vis *18*, 14. 10.1167/18.13.14.
31. Burr, D., Binda, P., and Gori, M. (2012). Multisensory Integration and Calibration in Adults and in Children 10.1093/acprof:oso/9780195387247.003.0010.
32. Bridge, H., Leopold, D.A., and Bourne, J.A. (2016). Adaptive Pulvinar Circuitry Supports Visual Cognition. Trends Cogn Sci *20*, 146-157. 10.1016/j.tics.2015.10.003.
33. Binda, P., Kurzawski, J.W., Lunghi, C., Biagi, L., Tosetti, M., and Morrone, M.C. (2018). Response to short-term deprivation of the human adult visual cortex measured with 7T BOLD. Elife *7*. 10.7554/eLife.40014.
34. Kurzawski, J.W., Lunghi, C., Biagi, L., Tosetti, M., Morrone, M.C., and Binda, P. (2022). Short-term plasticity in the human visual thalamus. Elife *11*. 10.7554/eLife.74565.
35. Goebel, R., Esposito, F., and Formisano, E. (2006). Analysis of functional image analysis contest (FIAC) data with brainvoyager QX: From single-subject to cortically aligned group general linear model analysis and self-organizing group independent component analysis. Hum Brain Mapp *27*, 392-401. 10.1002/hbm.20249.
36. Fischl, B., Salat, D.H., Busa, E., Albert, M., Dieterich, M., Haselgrove, C., van der Kouwe, A., Killiany, R., Kennedy, D., Klaveness, S., et al. (2002). Whole brain segmentation: automated labeling of neuroanatomical structures in the human brain. Neuron *33*, 341-355. 10.1016/s0896-6273(02)00569-x.
37. Jenkinson, M., Beckmann, C.F., Behrens, T.E., Woolrich, M.W., and Smith, S.M. (2012). Fsl. Neuroimage *62*, 782-790. 10.1016/j.neuroimage.2011.09.015.
38. Tustison, N.J., and Avants, B.B. (2013). Explicit B-spline regularization in diffeomorphic image registration. Front Neuroinform *7*, 39. 10.3389/fninf.2013.00039.
39. Mazziotta, J., Toga, A., Evans, A., Fox, P., Lancaster, J., Zilles, K., Woods, R., Paus, T., Simpson, G., Pike, B., et al. (2001). A probabilistic atlas and reference system for the human brain: International Consortium for Brain Mapping (ICBM). Philos Trans R Soc Lond B Biol Sci *356*, 1293-1322. 10.1098/rstb.2001.0915.
40. Jezzard, P., and Balaban, R.S. (1995). Correction for geometric distortion in echo planar images from B0 field variations. Magn Reson Med *34*, 65-73. 10.1002/mrm.1910340111.
41. Rushmore, R.J., Sunderland, K., Carrington, H., Chen, J., Halle, M., Lasso, A., Papadimitriou, G., Prunier, N., Rizzoni, E., Vessey, B., et al. (2022). Anatomically curated segmentation of human subcortical structures in high resolution magnetic resonance imaging: An open science approach. Front Neuroanat *16*, 894606. 10.3389/fnana.2022.894606.

42. Kasper, L., Bollmann, S., Diaconescu, A.O., Hutton, C., Heinzle, J., Iglesias, S., Hauser, T.U., Sebold, M., Manjaly, Z.M., Pruessmann, K.P., and Stephan, K.E. (2017). The PhysIO Toolbox for Modeling Physiological Noise in fMRI Data. J Neurosci Methods *276*, 56-72. 10.1016/j.jneumeth.2016.10.019.
43. Cieslak, M., Cook, P.A., He, X., Yeh, F.C., Dhollander, T., Adebimpe, A., Aguirre, G.K., Bassett, D.S., Betzel, R.F., Bourque, J., et al. (2021). QSIPrep: an integrative platform for preprocessing and reconstructing diffusion MRI data. Nat Methods *18*, 775-778. 10.1038/s41592-021-01185-5.
44. Benjamini, Y., and Hochberg, Y. (1995). Controlling the False Discovery Rate: A Practical and Powerful Approach to Multiple Testing. Journal of the Royal Statistical Society: Series B (Methodological) *57*, 289–300. https://doi.org/10.1111/j.2517-6161.1995.tb02031.x.
45. Frassle, S., Lomakina, E.I., Kasper, L., Manjaly, Z.M., Leff, A., Pruessmann, K.P., Buhmann, J.M., and Stephan, K.E. (2018). A generative model of whole-brain effective connectivity. Neuroimage *179*, 505-529. 10.1016/j.neuroimage.2018.05.058.
46. Frassle, S., Lomakina, E.I., Razi, A., Friston, K.J., Buhmann, J.M., and Stephan, K.E. (2017). Regression DCM for fMRI. Neuroimage *155*, 406-421. 10.1016/j.neuroimage.2017.02.090.
47. Frassle, S., Harrison, S.J., Heinzle, J., Clementz, B.A., Tamminga, C.A., Sweeney, J.A., Gershon, E.S., Keshavan, M.S., Pearlson, G.D., Powers, A., and Stephan, K.E. (2021). Regression dynamic causal modeling for resting-state fMRI. Hum Brain Mapp *42*, 2159-2180. 10.1002/hbm.25357.